

Luminescent properties of $\text{SrLi}_3\text{AlO}_4:\text{Eu}^{2+}$ phosphor with two narrow-band emissions discovered by the single-particle-diagnosis approach

Hiroaki Toyoshima, Takayuki Nakanishi, Jian Xu, Shiro Funahashi, Kohsei Takahashi, Hideyuki Emoto, Naoto Hirosaki & Koji Morita

To cite this article: Hiroaki Toyoshima, Takayuki Nakanishi, Jian Xu, Shiro Funahashi, Kohsei Takahashi, Hideyuki Emoto, Naoto Hirosaki & Koji Morita (2026) Luminescent properties of $\text{SrLi}_3\text{AlO}_4:\text{Eu}^{2+}$ phosphor with two narrow-band emissions discovered by the single-particle-diagnosis approach, Science and Technology of Advanced Materials, 27:1, 2650843, DOI: [10.1080/14686996.2026.2650843](https://doi.org/10.1080/14686996.2026.2650843)

To link to this article: <https://doi.org/10.1080/14686996.2026.2650843>



© 2026 The Author(s). Published by National Institute for Materials Science in partnership with Taylor & Francis Group.



[View supplementary material](#)



Published online: 09 Apr 2026.



[Submit your article to this journal](#)



Article views: 163



[View related articles](#)



[View Crossmark data](#)

Luminescent properties of $\text{SrLi}_3\text{AlO}_4\text{:Eu}^{2+}$ phosphor with two narrow-band emissions discovered by the single-particle-diagnosis approach

Hiroaki Toyoshima ^{a,b}, Takayuki Nakanishi ^c, Jian Xu ^{d,e,f}, Shiro Funahashi ^c, Kohsei Takahashi ^c, Hideyuki Emoto^a, Naoto Hiroaki ^c and Koji Morita ^{b,c}

^aDenka Co. Ltd, Machida, Tokyo, Japan;

^bGraduate School of Engineering, Kyushu University, Fukuoka, Japan;

^cResearch Center for Electronic and Optical Materials, National Institute for Materials Science(NIMS), Tsukuba, Ibaraki, Japan;

^dInternational Center for Young Scientists (ICYS), National Institute for Materials Science (NIMS), Tsukuba, Ibaraki, Japan;

^eGraduate School of Human and Environmental Studies, Kyoto University, Kyoto, Japan;

^fGraduate School of Global Environmental Studies (GSGES), Kyoto University, Kyoto, Japan

ABSTRACT

Phosphors exhibiting narrow-band emission are key materials for LED backlights in next-generation liquid crystal displays (LCDs) that require high color reproducibility. We successfully realized a hypothetical composition, $\text{SrLi}_3\text{AlO}_4$ (SLAO): Eu^{2+} , which is expected to exhibit narrow-band emission, by inspiring from reported $\text{SrLiAl}_3\text{N}_4$ (SLAN): Eu^{2+} . Using a single-particle-diagnosis approach, SLAO was selectively extracted from calcined powder mixture involving multiple phases, followed by crystal structure analysis and optical property characterization. SLAO:Eu has a similar cubic structure as SLAN, while it shows narrow-band yellow-green emission at 521 nm and 567 nm with full widths at half maximum (FWHM) of 39 nm and 40 nm, respectively. The emission characteristic is comparable with that of quantum dots, demonstrating (i) the feasibility of material design based on the coordination environment similarities and (ii) the resultant SLAO:Eu as a promising phosphor for the next-generation display applications.

ARTICLE HISTORY

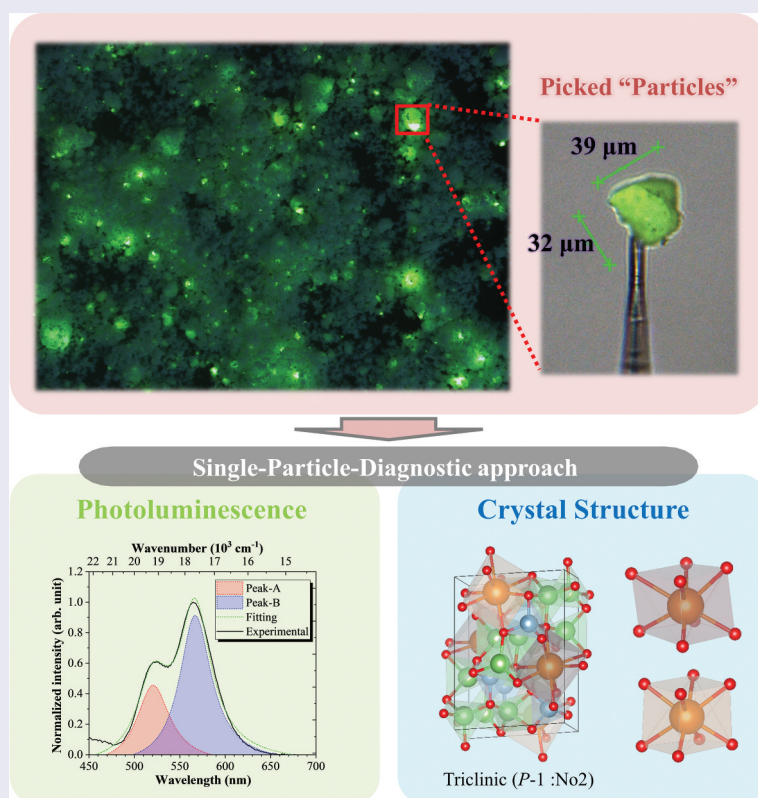
Received 12 December 2025



Revised 10 February 2026


Accepted 20 March 2026

KEYWORDS

Phosphor; narrow-band emission; white LED; LCD display



CONTACT Takayuki Nakanishi  Nakanishi.Takayuki@nims.go.jp  Research Center for Electronic and Optical Materials, National Institute for Materials Science(NIMS), 1-1 Namiki, Tsukuba, Ibaraki 305-0044, Japan

 Supplemental data for this article can be accessed online at <https://doi.org/10.1080/14686996.2026.2650843>

© 2026 The Author(s). Published by National Institute for Materials Science in partnership with Taylor & Francis Group.

This is an Open Access article distributed under the terms of the Creative Commons Attribution License (<http://creativecommons.org/licenses/by/4.0/>), which permits unrestricted use, distribution, and reproduction in any medium, provided the original work is properly cited. The terms on which this article has been published allow the posting of the Accepted Manuscript in a repository by the author(s) or with their consent.

IMPACT STATEMENT

Discovery of unreported $\text{SrLi}_3\text{AlO}_4\text{:Eu}^{2+}$ with two narrow emission bands via single-particle-diagnosis, demonstrating an innovative approach for designing novel high-performance phosphors

1. Introduction

Phosphors exhibiting narrow emission bands serve as key materials for LED backlights used in high-performance liquid crystal displays (LCDs) [1,2]. Since the color reproduction range of LCDs corresponds to the wavelength range that can be reproduced by the blue, green, and red lights extracted from a white LED – which combines blue LEDs and phosphors – through color filters thus requiring phosphors with narrow-band emission. For high-end typed displays with high color reproducibility, the blue emission is provided by blue LEDs and the red emission utilizes $\text{K}_2\text{SiF}_6\text{:Mn}^{4+}$ (KSF; FWHM \approx 5 nm, peaked at 630 nm) [3]. In addition, the green emission utilizes $\text{Si}_{6z}\text{Al}_z\text{O}_z\text{N}_{8x}\text{:Eu}^{2+}$ (β -SiAlON, FWHM = 55 nm, peaked at 535 nm) [4,5], $\text{SrGa}_2\text{S}_4\text{:Eu}^{2+}$ (SGS, FWHM = 50 nm, peaked at 540 nm) [6] and quantum dots [7–9].

To fulfill the specifications required for next-generation 8k displays, new material designs are needed that enable novel green phosphors with greater stability and narrower emission bandwidths (≤ 50 nm) as compared to currently available green phosphors, such as β -SiAlON. As one of the potential candidates, narrow emission bandwidths can be realized by Eu^{2+} -activated phosphors exhibiting strong absorption in the blue region, which can be attributed to $4f$ - $5d$ spin/parity-allowed electronic transitions. As a notable example, Schnick *et al.* [10] reported that $\text{SrLiAl}_3\text{N}_4$ (SLAN): Eu^{2+} , in which Eu^{2+} is substituted into highly symmetric cubic coordination environments, yields an extremely narrow emission band (FWHM: 50 nm, peaked at 650 nm) in red. Similar emission characteristics can generally be expected to be attained in similar coordination environments. Indeed, other nitride and oxide phosphors with the crystal structures similar to SLAN, which belongs to the UCr_4C_4 -type family [11], have also been reported to exhibit narrow emission bands [12–16]. Furthermore, in order to enable efficient exploration of new phosphors, we have employed material informatics (MI) focusing on ideal coordination geometries and successfully reported new phosphors with narrow-band emission in the ultraviolet–blue region [17–19]. By employing Wasserstein (WS) distance as a typical MI index, it is possible to quantitatively evaluate the similarity between the coordination environments of phosphors with narrow emission bandwidth and those registered in the inorganic crystal structure database (ICSD) [17]. Consequently, a new blue phosphor $\text{K}_2\text{ZnP}_2\text{O}_7\text{:Eu}^{2+}$ with an emission

peak at 440 nm and FWHM of 30 nm was successfully developed [19].

Herein, in order to realize novel Eu^{2+} -activated phosphors with narrow-band emissions, an effective exploration method is the ionic substitution approach based on framework structures with focus on the similarity of local coordination environments. In this study, we focused on the hitherto unreported hypothetical composition $\text{SrLi}_3\text{AlO}_4$, which can be obtained by substituting O for N in the SLAN:Eu phosphor as a design concept. The hypothetical composition $\text{SrLi}_3\text{AlO}_4$ is an ideal structure obtained by complete substitution, where Al^{3+} is replaced by Li^+ , and N^{3-} by O^{2-} , to maintain charge balance. Based on the crystal structure of SLAN, it is expected to exhibit a narrow emission bandwidth. In particular, since replacing N^{3-} with O^{2-} lowers the covalency, it can be expected to suppress the nephelauxetic effect on the splitting of the $5d$ orbital of Eu^{2+} , and, hence, to give emission in shorter wavelength regions rather than SLAN:Eu $^{2+}$ in red [20,21]. Although SLAO:Eu $^{2+}$ is expected to exhibit visible emission with a narrow bandwidth, there are no reports of successful synthesis for this compound.

In this study, a single-particle-diagnosis approach [22], which enables crystal structure analysis and optical property evaluation at the submicron particle level, is adopted to clarify the synthesis of SLAO:Eu $^{2+}$. The single-particle-diagnosis approach enables selective extraction of individual particles from powder mixture involving multiple phases, followed by crystal structure and optical property characterization. This method allows for high-precision exploration and evaluation of phases that tend to be neglected in conventional approaches due to low light yield under nonoptimized synthesis conditions [23–26]. By applying the single-particle-diagnosis approach, highly accurate verification of the synthesis of SLAO:Eu $^{2+}$ was achieved, resulting in the realization of uniquely narrow emission bandwidth that are rarely observed among existing phosphors. This paper reports the realization of the SLAO phosphor with two narrow emission peaks in the green and yellow regions.

2. Experimental section

2.1. Sample preparation

$\text{Sr}_{0.99}\text{Eu}_{0.01}\text{Li}_3\text{AlO}_4$ was synthesized by the conventional solid-state reaction method. SrO (98%, High

Purity Chem. Lab. Co., Ltd.), Li_2O (99.9%, High Purity Chem. Lab. Co., Ltd.), LiAlO_2 (99.9%, High Purity Chem. Lab. Co., Ltd.), and Eu_2O_3 (99.9%, Shin-Etsu Chemical Co., Ltd.) were used as starting raw materials. Li_2O and SrO were selected to avoid insufficient decarbonation, and LiAlO_2 was employed because Al_2O_3 was expected to remain unreacted due to its low reactivity. The raw powders were weighed in a glove box filled with nitrogen gas to achieve a molar ratio of $\text{Sr}:\text{Li}:\text{Al}:\text{Eu} = 0.99:3:1:0.01$, and then thoroughly mixed within an alumina mortar. The powder mixture was placed into an alumina boat and heated to 800°C at a rate of $10^\circ\text{C}/\text{min}$ in a tube furnace under ammonia gas flow, followed by calcination for 8 h. The calcined sample was ground in the air using an alumina mortar.

2.2. Single-particle extraction and characterization

The crystalline phases of the synthesized sample were confirmed by powder X-ray diffraction (Ultima IV, Rigaku). The composition of the synthesized sample was confirmed by inductively coupled plasma emission spectroscopy (CIROS-120, SPECTRON). The synthesized sample was illuminated with a 365-nm UV-LED lamp to excite the particles. Emitting particles were observed using an optical camera and selectively collected onto the tip of a glass capillary using epoxy resin. The crystal phases of the collected luminescent single particles were identified by single-crystal X-ray diffractometer (XtaLab Synergy-Custom, Rigaku), using $\text{Mo K}\alpha$ radiation ($\lambda = 0.71073 \text{ \AA}$) at 45 kV and 66 mA. Diffraction intensity integration calculations and absorption correction were performed using *CrysAlisPro*. Crystal structure was determined by using the *SHELX* program [27,28], followed by least-squares refinement. The composition ($\text{Sr}:\text{Al}$ molar ratio) of the single particles was confirmed by SEM-EDS (SU1510, Hitachi High-Tech and XFlash, Bruker) elemental analysis.

The single-particle photoluminescence (PL) spectra were measured using an apparatus consisting of a sample holder, excitation fiber, detection fiber, and a multichannel spectrometer [29]. The excitation source was a wavelength-tunable xenon lamp (SM-10ND2, Spectra Instruments) with a power of 150 W. Detection was performed using a multichannel photodetector (MCPD9800-3095, Otsuka Electronics), with a single-core fiber (core diameter $115 \mu\text{m}$) for excitation and a multicore band fiber ($200 \mu\text{m} \times 10$) for detection; the excitation-detection distance was set at $500 \mu\text{m}$. Quantum efficiency measurements of single particles were performed with a precise sample holder, excitation fiber, detection fiber, and multichannel spectrometer [30]. The sample holder was mounted on a three-axis goniometer head commonly used for

X-ray diffraction. The excitation wavelength was set to 440 nm. Emission was detected by rotating the sample holder with a motor to collect emissions from various directions. Time-resolved emission spectra were measured by an apparatus consisting of a Ti:sapphire laser with optical parametric generator (OPG) (Chameleon Vision-S, Coherent, Inc.), a high-resolution spectrometer (SpectraPro HRS-300, Princeton Instrument, Inc.), and a streak camera (C14831-110, Hamamatsu Photonics Co., Ltd.) [31]. Particles were placed on a copper plate and excited with a 455 nm, 75 fs pulse produced by the Ti:sapphire laser at an emission wavelength of 730 nm. Time resolution was measured up to 9 μs . Temperature dependence was measured using a microcryostat (Janis ST-500, Lake Shore Cryotronics, Inc.) at 80 K and from 100 to 600 K with 50 K intervals.

3. Results and discussion

3.1. Identification of $\text{SrLi}_3\text{AlO}_4:\text{Eu}^{2+}$ single particles

In order to identify the crystalline phases formed in the calcined powder sample, XRD measurements were performed. Figure 1(a) shows the powder X-ray diffraction pattern of the as-calcined $\text{SrLi}_3\text{AlO}_4:\text{Eu}^{2+}$ sample, including the measured data (open circles), calculated profile (red line), and their difference (green line). The peak markers indicate $\text{Sr}_2\text{LiAlO}_4$ (\bullet) and Li_5AlO_4 (\blacktriangle). The main phases of the calcined powder are Li_5AlO_4 (PDF4+(ICDD)-04-010-8876, 46 wt%) and $\text{Sr}_2\text{LiAlO}_4$ (PDF4+(ICDD)-04-026-1870, 54 wt%) [32]. In addition to these two dominant phases, very weak peaks of unknown phases are observed around 16° and 38° . The obtained reliability factors are $R_{\text{wp}} = 8.93\%$ and $R_p = 6.36\%$, confirming these two phases as the main compositions. Since Li tends to volatilize during the calcination, which might alter the composition, quantitative analysis of the element ratio in the calcined powder was conducted by ICP emission spectroscopy. After the calcination, the composition was $\text{Li}:\text{Sr}:\text{Al}:\text{Eu} = 3.05:0.99:1.03:0.01$. Comparing this to the nominal composition before the calcination ($\text{Li}:\text{Sr}:\text{Al}:\text{Eu} = 3.00:0.99:1.00:0.01$), the variation of Li and Al is less than 0.05, indicating negligible deviation from stoichiometry.

To investigate the distribution and emission color of the luminescent particles in the powder, the sample was illuminated with a 365-nm UV lamp and observed by a fluorescence microscope. Figure 1(b) shows the fluorescence images of the crystalline particles from the as-calcined powders just after synthesis and after 2 weeks' exposure in the air atmosphere, respectively. Red arrows indicate strong yellow-green luminescent particles focused on this study. The X-ray diffraction pattern of the sample after the two-week exposure is

shown in **Figure S1**. Immediately after the synthesis, three types of particles were observed: nonluminescent, weak yellow-green emitting, and strong yellow-green emitting. After 2 weeks, only the strong yellow-green emitting particles remain, while the emission from the weak-yellow-green particles disappeared. Comparing the images under the visible light and UV irradiations, most particles are nonluminescent or weakly luminescent, and only a minority are strongly luminescent. It is also confirmed that the $\text{Sr}_2\text{LiAlO}_4$ host lattice without Eu^{2+} did not exhibit any luminescence, suggesting that it exhibits no defect-related luminescence. According to the report by Hoerder *et al.*, $\text{Sr}_2\text{LiAlO}_4:\text{Eu}^{2+}$ shows green emission [32]. Based on the phase ratios from the XRD result, the nonluminescent

particles are assigned to Li_5AlO_4 , where Eu incorporation is disfavored due to the ionic radius and valence mismatch with $\text{Li}^+/\text{Al}^{3+}$; meanwhile the weak yellow-green emitting particles are presumed to be the previously reported $\text{Sr}_2\text{LiAlO}_4:\text{Eu}^{2+}$.

Figure 1(c) shows the single particle picked up and the apparatus employed for the single-particle photoluminescence analysis. **Figure 1(d)** shows the obtained emission spectrum of a collected single particle with strong yellow-green emitting feature. The red dashed line represents the deconvoluted spectrum of the fitted Peak-A component, while the blue dashed line corresponds to the deconvoluted spectrum of the fitted Peak-B component. The green dashed line indicates the fitted spectrum obtained by summing Peaks A and

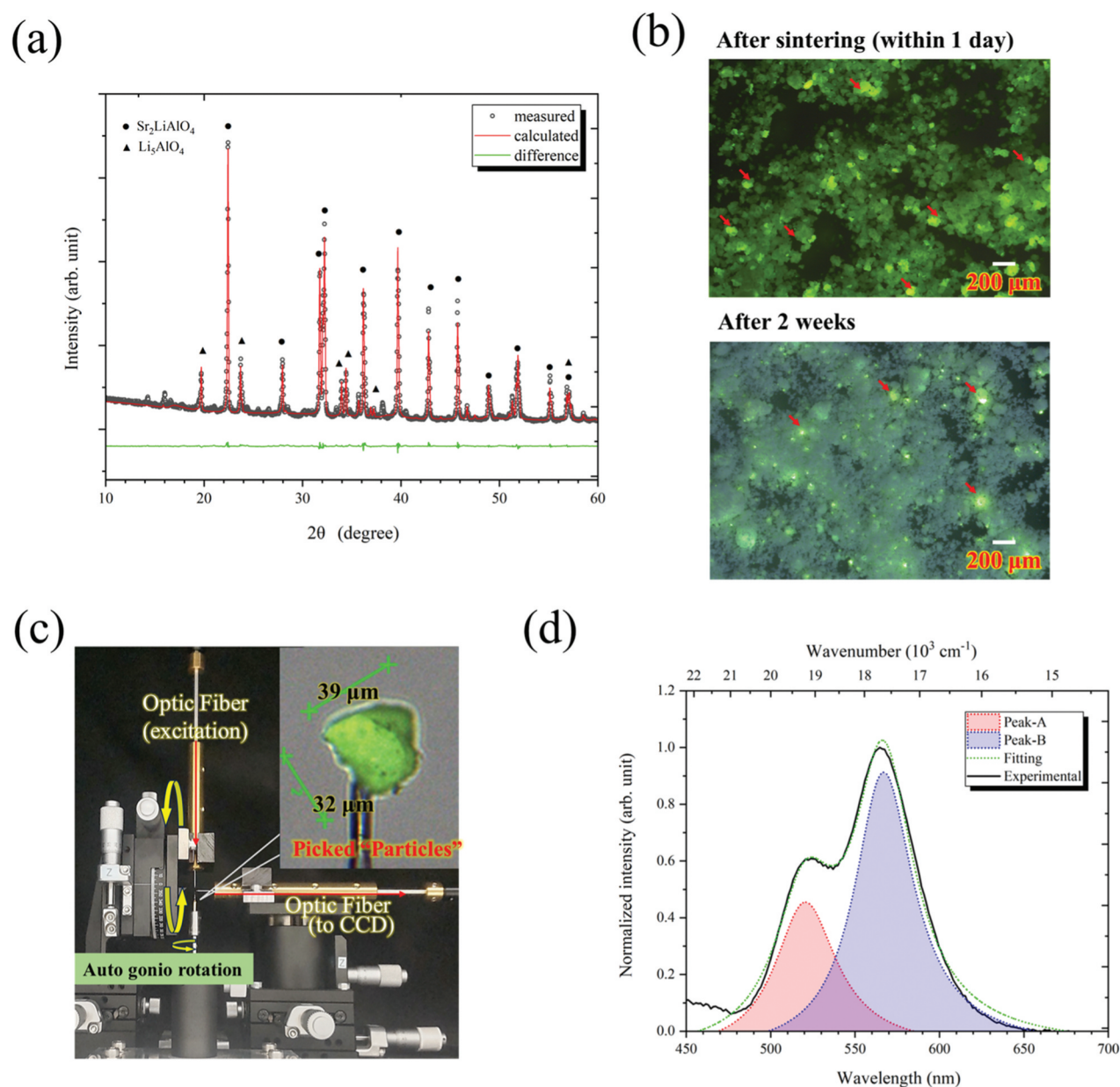


Figure 1. (a) Powder X-ray diffraction pattern of $\text{SrLi}_3\text{AlO}_4:\text{Eu}^{2+}$ as-calcined sample. (b) Fluorescence microscope image ($\lambda_{\text{ex}} = 365 \text{ nm}$) of the calcined powder sample (immediately after calcination) and the sample observed two weeks later. (c) The single particle picked up and the apparatus for single particle photoluminescence and IQE measurements. (d) Single-particle emission spectrum of yellow-green luminescent particle ($\lambda_{\text{ex}} = 402 \text{ nm}$) and its Lorentzian fitting on spectrum (fitting approach was performed in the energy scale, cm^{-1} for X-axis).

B, and the black solid line shows the experimental emission spectrum.

The spectrum displays two peaks: the subpeak A at around 520 nm and the main peak B at around 570 nm by the Lorentzian fitting after converting the wavelength to wavenumber. The calculated emission peak wavelengths are 521 nm (FWHM: 39 nm) for the subpeak A and 567 nm (FWHM: 40 nm) for the main peak B. FWHM values of each emission band are approximately about 20% narrower than that of β -SiAlON [4,5]. This suggests that if the two emission bands could successfully be separated into each band, this potentially enable to realize excellent color purity.

3.2. Crystal structure analysis of $\text{SrLi}_3\text{AlO}_4\text{:Eu}^{2+}$ single particles

Figure 2(a) shows the crystal structure of SLAO determined by single-particle-diagnosis approach [22]. The structure consists of SrO_8 cuboid-like polyhedron with Sr coordinated by eight O atoms, and $\text{AlO}_4/\text{LiO}_4$ tetrahedra sharing edges. The refined parameters and atomic coordinates are listed in Tables S1 and S2. The crystal structure belongs to the triclinic system, space group $P\bar{1}$ (No. 2), with

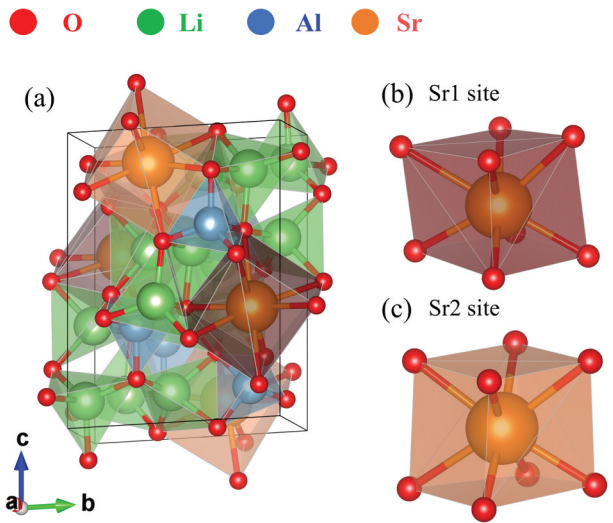


Figure 2. (a) Crystal structure of $\text{SrLi}_3\text{AlO}_4\text{:Eu}^{2+}$ phosphor (red, green, blue, and orange spheres represent oxygen (O), lithium (Li), aluminum (Al), and strontium (Sr) atoms, respectively). (b) Local coordination environment around the Sr1 site. (c) Local coordination environment around the Sr₂ site. This crystal structure images were drawn with the program VESTA [33].

lattice constants of $a = 5.7375(3) \text{ \AA}$, $b = 7.3158(4) \text{ \AA}$, $c = 9.7025(5) \text{ \AA}$, $\alpha = 83.949(4)^\circ$, $\beta = 76.658(5)^\circ$, and $\gamma = 79.619(5)^\circ$. Reliability factors were $R = 2.72\%$, $wR2 = 5.42\%$, $\text{GOF} = 1.12$, indicating successful refinement. The composition estimated from the electron density distribution is confirmed to be $\text{SrLi}_3\text{AlO}_4$, matching well with the designed (hypothetical) composition but differing from the main phase $\text{Sr}_2\text{LiAlO}_4$. EDS analysis for the selected particle supported the assignment of $\text{SrLi}_3\text{AlO}_4$ (SLAO), with a Sr/Al ratio of 1.00:1.06 (at%). Table 1 compares the lattice parameters of SLAO and SLAN. It can be confirmed that both phases have identical crystal system and space group, and the axes lengths of SLAO are about 2–3% shorter than those of SLAN. Figure 2(b,c) shows the local coordination environments around the Sr1 and Sr2 sites, which can be characterized by cuboid-like eightfold coordination with O atoms similar to SLAN. Each SrO_8 cuboid-like polyhedron is stacked by face-sharing along $[0\ 1\ 1]$ axis (see Figure S2). The SLAO structure involves full substitution of the Li site with Al and vice versa, and N site with O, as compared to SLAN.

To quantitatively assess the similarity in the Sr site environments between SLAO and SLAN, Wasserstein (WS) distance [17] is calculated which can simply evaluate the similarity of the local coordination environments. The WS distance is defined by the following:

$$W(f,g) = \inf_{\pi \in \Gamma(f,g)} \int_{R \times R} c(x,y) d\pi(x,y), \tag{1}$$

where $c(x,y) = |x - y|$ is the transport distance cost matrix, and $\Gamma(f,g)$ denotes the set of all pairings of f and g with marginal distributions for the first and second factors, respectively. This value is ‘zero’ when the two local structures are geometrically similar. Using the Sr1 site within the SLAN as a reference, the WS distances of the Sr2 site within the SLAN and the Sr1 and Sr2 sites within the SLAO are calculated, as shown in Table 2. The WS distance between the Sr2 site and the Sr1 site in SLAN is a very small value of 0.016, leading to the conclusion that their respective coordination environments possessed a high degree of similarity [17]. The WS distances for the Sr1 and Sr2 sites in SLAO were 0.022 and 0.021, respectively. These values are also small, indicating that the Sr1 and Sr2 sites in SLAO possessed coordination

Table 1. Lattice constants of $\text{SrLi}_3\text{AlO}_4$ (SLAO) and $\text{SrLiAl}_3\text{N}_4$ (SLAN) structures.

		SLAO	SLAN [10]	Difference SLAO/SLAN
Crystal system		Triclinic	Triclinic	
Space group		$P\bar{1}$	$P\bar{1}$	
Cell parameters (Å)	a	5.75375(3)	5.86631(12)	98.1%
	b	7.3158(4)	7.51099(15)	97.4%
	c	9.7025(5)	9.96545(17)	97.4%
Cell angle (°)	α	83.949(4)	83.6028(12)	–
	β	76.658(5)	76.7720(13)	–
	γ	79.619(5)	79.5650(14)	–

Table 2. Wasserstein distance calculated using the Sr1 site of $\text{SrLiAl}_3\text{N}_4$ (SLAN) as the reference.

Composition	Site	Wasserstein distance
SLAN	Sr1	0.000*
	Sr2	0.016
SLAO	Sr1	0.022
	Sr2	0.021

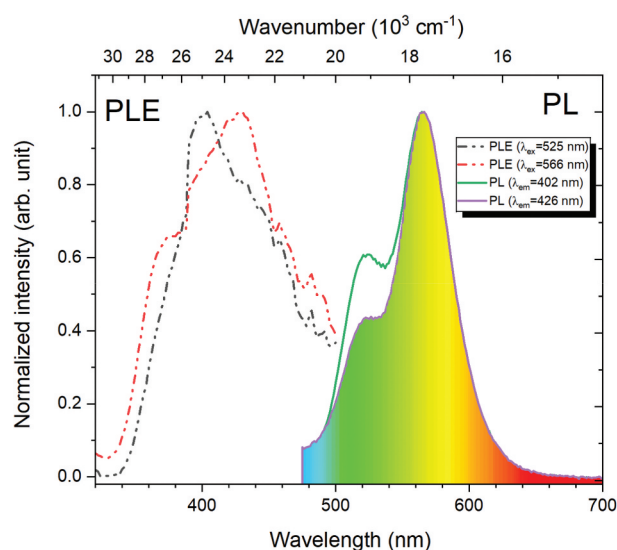
*As a reference.

environments highly similar to that of SLAN. These results suggest that the narrow-band emission of SLAO can be ascribed to this similarity in the coordination environment with SLAN.

Although the WS distance is an excellent indicator of the coordination environment similarity, it does not account for bond distances. Comparison of the average Sr–O bond distances in SLAO (Sr1: 2.647 Å, Sr2: 2.678 Å) with those of Sr–N in SLAN (Sr1: 2.797 Å, Sr2: 2.803 Å) shows that SLAO has about 5% shorter anion distances (see in **Table S3**). This should ordinarily result in a stronger crystal field splitting of Eu^{2+} 5d orbitals, shifting the emission to longer wavelengths. In contrast, however, the main emission peak of SLAO (567 nm) was found at shorter wavelengths than that of SLAN (650 nm), suggesting that both the reduced covalency and suppressed nephelauxetic effect decrease the splitting of Eu^{2+} :5d orbitals [20,21].

3.3. Photoluminescence properties of SLAO:Eu single particles

Phosphors for white LED applications are required to possess high quantum efficiency and efficiently absorption coefficient matching with emission curves of commercial LEDs. Furthermore, since the heat caused from the blue LED chip is transferred to the resin layer where the phosphor is dispersed, the phosphor temperature itself can easily reach above 100°C.

**Figure 3.** PLE ($\lambda_{\text{em}} = 525$ nm, 566 nm) and PL spectra ($\lambda_{\text{ex}} = 402$ nm, 426 nm) of the $\text{SrLi}_3\text{AlO}_4\text{:Eu}^{2+}$ single particle.

Therefore, it is essential that the luminescence intensity should not decrease significantly with increasing temperature.

Figure 3 shows the PLE ($\lambda_{\text{em}} = 525$ nm, 566 nm) and PL spectra ($\lambda_{\text{ex}} = 402$ nm, 426 nm) of the SLAO:Eu single particle in which the two emission bands (subband A and main-band B) are suggested to correspond to the two different Sr sites indicated by the above crystal structure analysis. According to the report by Bouquiaux et al., Eu^{2+} can occupy both the Sr1 and Sr2 sites in $\text{SrLiAl}_3\text{N}_4\text{:Eu}^{2+}$, their emissions exhibit closely spaced zero-phonon-line energies and strongly overlapping vibronic envelopes. Furthermore, the intrinsically broader Sr2-centered emission effectively masks the narrower Sr1 contribution, resulting in a single apparent emission band [34]. In contrast, the ZPL positions and vibronic overlap in SALO differ from those in SLA, which likely leads to the observation of two distinct emission bands.

The excitation spectrum extends widely to the visible region, suggesting strong absorption of UV–blue light and high compatibility with commercial LED light sources, in particular, the 450 nm one. **Figure S3** shows the emission spectrum for the quantum efficiency measurement of a single SLAO particle, where BaSO_4 powders were used as reference. The calculated internal quantum efficiency (IQE) of the SLAO:Eu single particle is ~46%. **Figure S4** displays the temperature dependence of the integrated emission intensity, normalized to the value at 303 K (30°C). The integrated emission intensity decreased linearly with increasing temperature, dropping to ~80% at 403 K and ~60% at 503 K relative to the value at 303 K. Note that the emission intensity of the single particle may strongly change due to slight moving of sample position during the heating. Therefore, we examine its temperature dependence of fluorescence lifetime monitoring both radiative and non-radiative dynamics of the Eu^{2+} excited state, which gives more intrinsic information than the PL intensity.

Figure 4(a) shows the streak images of the SLAO:Eu single particle recorded from 80 K to 600 K by 455 nm laser excitation. Detailed analytical results of the streak imaging can be found in **Figure S5** taking the temperature conditions at 80 K, 200 K, 400 K, and 600 K as typical examples. Judging from the temperature evolution of the time-resolved spectroscopy from 80 K to 600 K, the emission band of SLAO:Eu can generally be divided into two components involving the subband A (490–540 nm) with a shorter lifetime and the main-band B (540–650 nm) with a longer lifetime. It is worth noting that these is no obvious change for the lifetime even up to 600 K for both two emission components, while slight peak broadening can be observed at a monitoring temperature of 600 K as compared to that at 80 K. **Figure 4(b,c)** presents normalized

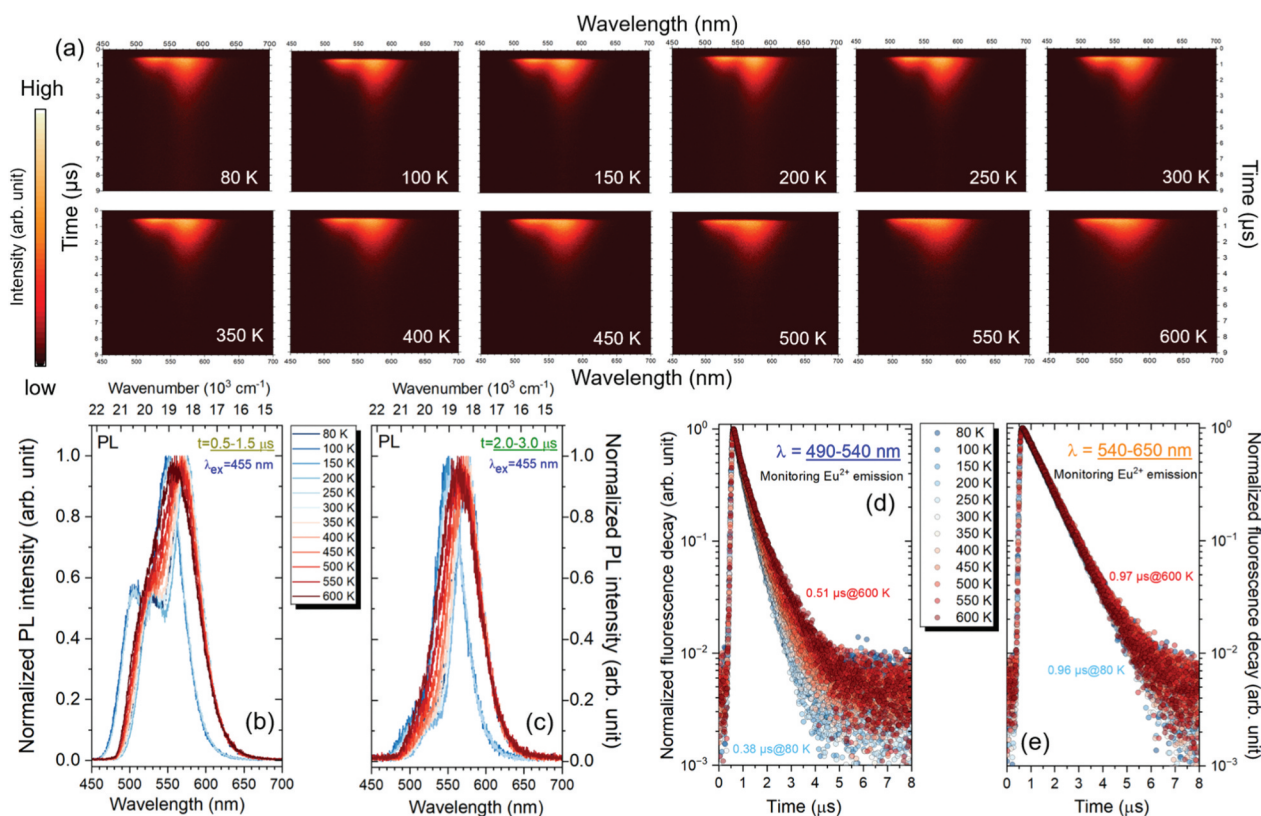


Figure 4. (a) Temperature dependence of time-resolved streak imaging of SrLi₃AlO₄:Eu²⁺ single-particle phosphor from 80 K to 600 K; normalized PL spectra ($\lambda_{\text{ex}} = 455$ nm) between (b) 0.5 and 1.5 μs , (c) 2.0 and 3.0 μs ; normalized fluorescence decay curves monitoring the wavelength region of (d) 490–540 nm and (e) 540–650 nm.

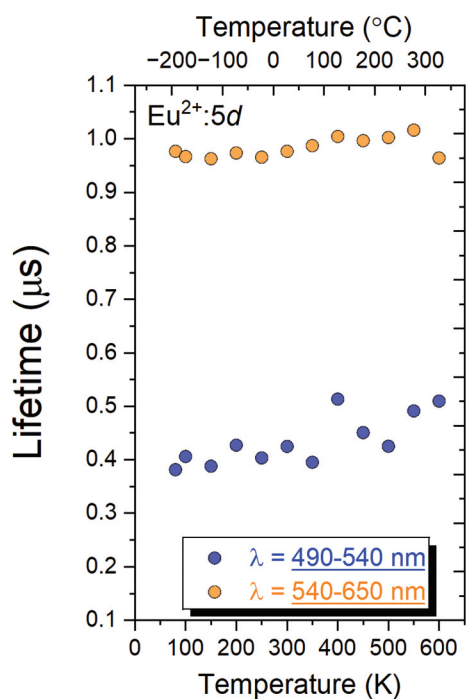


Figure 5. Temperature dependence of estimated fluorescence lifetime monitoring the wavelength region of 490–540 nm and 540–650 nm, respectively.

emission spectra at different temperatures for the 0.5–1.5- μs and 2.0–3.0- μs interval, respectively, which indicates the broadening mainly occurs for the short-time interval, while the dominant main-

band B only shifts to longer wavelength when temperature increases from 80 K to 600 K. On the other hand, the normalized fluorescence decay curves monitoring the subband A and the main-band B are shown in Figure 4(d,e), respectively. The estimated lifetimes of the two emission regions monitored at different temperatures are summarized in Figure 5. The fluorescence lifetime in the wavelength region dominated by the sub-band A (490–540 nm) is estimated to be $\sim 0.4 \mu\text{s}$ and increases gradually with temperature up to 550 K. The relatively lifetime increase monitored at the wavelength range of the subband A is partially due to the mixing of the main-band B (540–650 nm) by inhomogeneous broadening at high temperatures. On the other hand, the fluorescence lifetime in the region dominated by the main-band B (540–650 nm) is estimated to be $\sim 1.0 \mu\text{s}$ at 80 K and remains almost unchanged as temperature increases, indicating extremely high thermal stability of this material with very limited nonradiative contribution even up to 600 K. Furthermore, the distinct fluorescence lifetimes of subband A and main-band B suggests that an energy-transfer process from subband A to main-band B may be operative. As the present evaluation was performed on a single particle, more detailed investigations using single-phase bulk powder samples will be necessary in the future work.

4. Conclusion

A novel $\text{SrLi}_3\text{AlO}_4$ (SLAO): Eu^{2+} phosphor exhibiting ultranarrow yellow-green emission bands was discovered for the first time using a single-particle-diagnosis approach. This advanced phosphor screening technique enabled selective extraction and precise analysis of individual particles with submicron size from multiphase powder samples, allowing for accurate crystal structure determination and optical characterization. It is, generally, quite challenging by other screening methods, especially for minor phases involved. As a consequence, the SLAO: Eu^{2+} phosphor was confirmed to have two emission peaks at 521 nm and 567 nm with exceptionally narrow FWHM of 39 nm and 40 nm, respectively, which are comparable with those of the quantum dots. Temperature dependence of time-resolved spectroscopy revealed superior thermal quenching behavior of SLAO: Eu^{2+} with very limited nonradiative contribution even up to 600 K. These results highlight the effectiveness of the single-particle-diagnosis approach for exploring new compounds and achieving high-performance narrow-band phosphors. Further material design efforts toward phase purity and single-band emission in the form of powder samples are expected to expand its potential for next-generation display applications.

Acknowledgments

This work was partially supported by Grant-in-Aid for Grant Number 24K01589. This work was partially supported by Innovative Science and Technology Initiative for Security Grant Number JPJ004596, ATLA, Japan.

Author contribution

CRedit: **Hiroaki Toyoshima**: Sample preparation, data collection, data analysis, and writing-original draft; **Takayuki Nakanishi**: Data collection, data analysis, writing-review, and editing; **Jian Xu**: Data analysis; S.F.: Crystal structure data collection and its analysis; **Kohsei Takahashi**: Photophysical properties' measurements for single particles; **Hideyuki Emoto**: Formal analysis; **Naoto Hirosaki**: Formal analysis; **Koji Morita**: Data collection, data analysis, writing – review and editing.

Disclosure statement

No potential conflict of interest was reported by the author(s).

Funding

The work was supported by the Japan Society for the Promotion of Science [24K01589]; Innovative Science and Technology Initiative for Security [JPJ004596].

ORCID

Hiroaki Toyoshima  <http://orcid.org/0009-0000-0866-4475>
 Takayuki Nakanishi  <http://orcid.org/0000-0003-3412-2842>
 Jian Xu  <http://orcid.org/0000-0002-1040-5090>
 Shiro Funahashi  <http://orcid.org/0000-0002-9381-3603>
 Kohsei Takahashi  <http://orcid.org/0000-0002-6443-1534>
 Naoto Hirosaki  <http://orcid.org/0000-0001-9218-9557>
 Koji Morita  <http://orcid.org/0000-0001-6040-7054>

References

- [1] Bando K, Noguchi Y, Sakamoto K, et al. Development and application of high-brightness white LEDs. In: Proc. Phosphor Res. Soc. 264th Meeting 1996; 264: 5-14; 1996.
- [2] Nakamura S, Fasol G. The blue laser diode: GaN based light emitters and lasers. Berlin: Springer-Verlag; 1997.
- [3] Takahashi T, Adachi S. Mn^{4+} -activated red photoluminescence in K_2SiF_6 phosphor. J Electrochem Soc. 2008;155(12):E183–E188.
- [4] Hirosaki N, Xie RJ, Kimoto K, et al. M. Appl Phys Lett. 2005;86(21):211905. doi: 10.1063/1.1935027
- [5] Takahashi K, Xie RJ, Hirosaki N. Toward higher color purity and narrower emission band β - SiAlON : eu^{2+} by reducing the oxygen concentration. Electrochem Solid-State Lett. 2011;14(11):E38–E40. doi: 10.1149/2.017111esl
- [6] Chartier C, Barthou C, Benalloul P, et al. Photoluminescence of Eu^{2+} in SrGa_2S_4 . J Lumin. 2005;111(3):147–158. doi: 10.1016/j.jlumin.2004.07.006
- [7] Chen O, Zhao J, Chauhan V, et al. Compact high-quality CdSe–CdS core–shell nanocrystals with narrow emission linewidths and suppressed blinking. Nat Mater. 2013;12(5):445–451. doi: 10.1038/nmat3539
- [8] Tamang S, Lincheneau C, Hermans Y, et al. Chemistry of InP nanocrystal syntheses. Chem Mater. 2016;28(8):2491–2506. doi: 10.1021/acs.chemmater.5b05044
- [9] Protesescu L, Yakunin S, Bodnarchuk MI, et al. Nanocrystals of cesium lead halide perovskites (CsPbX_3 , X = Cl, Br, and I): novel optoelectronic materials showing bright emission with wide color gamut. Nano Lett. 2015;15(6):3692–3696. doi: 10.1021/nl5048779
- [10] Pust P, Weiler V, Hecht C, et al. Narrow-band red-emitting $\text{Sr}[\text{LiAl}_3\text{N}_4]$: eu^{2+} as a next generation LED-phosphor material. Nat Mater. 2014;13(9):891–896. doi: 10.1038/nmat4012
- [11] Behrens RK, Jeitschko W. UCr_4C_4 with filled MoNi_4 type structure. Monatsh Chem. 1987;118(1):43–50. doi: 10.1007/BF00810039
- [12] Li YQ, Delsing ACA, With G, et al. Luminescence properties of Eu^{2+} -activated alkaline-earth siliconoxynitride $\text{MSi}_2\text{O}_{2-\delta}\text{N}_{2+2/3\delta}$ (M = Ca, Sr, Ba): a promising class of novel LED conversion phosphors. Chem Mater. 2005;17(12):3242–3248. doi: 10.1021/cm050175d
- [13] Pust P, Wochnik AS, Baumann E, et al. $\text{Ca}[\text{LiAl}_3\text{N}_4]$: eu^{2+} – a narrow-band red-emitting nitridolithoaluminate. Chem Mater. 2014;26(11):3544–3549. doi: 10.1021/cm501162n

- [14] Schmichen S, Schneider H, Wagatha P, et al. Toward new phosphors for application in illumination-grade white pc-LEDs: the nitridomagnosilicates $\text{Ca}[\text{Mg}_3\text{SiN}_4]$: Ce^{3+} , $\text{Sr}[\text{Mg}_3\text{SiN}_4]$: Eu^{2+} , and $\text{Eu}[\text{Mg}_3\text{SiN}_4]$. *Chem Mater.* **2014**;26(8):2712–2719. doi: [10.1021/cm500610v](https://doi.org/10.1021/cm500610v)
- [15] Zhao M, Liao H, Ning L, et al. Next-generation narrow-band green-emitting $\text{RbLi}(\text{Li}_3\text{SiO}_4)_2$: Eu^{2+} phosphor for backlight display application. *Adv Mater.* **2018**;30(38):1802489. doi: [10.1002/adma.201802489](https://doi.org/10.1002/adma.201802489)
- [16] Hoerder GJ, Seibald M, Baumann D, et al. $\text{Sr}[\text{Li}_2\text{Al}_2\text{O}_2\text{N}_2]$: Eu^{2+} , a high performance red phosphor to brighten the future. *Nat Commun.* **2019**;10(1):1824. doi: [10.1038/s41467-019-09632-w](https://doi.org/10.1038/s41467-019-09632-w)
- [17] Takemura S, Takeda T, Nakanishi, et al. Dissimilarity measure of local structure in inorganic crystals using Wasserstein distance to search for novel phosphors. *Sci Technol Adv Mater.* **2021**;22(1):185–193. doi: [10.1080/14686996.2021.1899555](https://doi.org/10.1080/14686996.2021.1899555)
- [18] Takemura S, Koyama Y, Nakanishi, et al. Narrow-band emitting phosphor $\text{Na}_2\text{Cs}_2\text{Sr}(\text{B}_9\text{O}_{15})_2$: Eu^{2+} discovered from local structure similarity with sulfate phosphor. *J Phys Chem Lett.* **2022**;13(51):11878–11882. doi: [10.1021/acs.jpclett.2c02889](https://doi.org/10.1021/acs.jpclett.2c02889)
- [19] Takemura S, Koyama Y, Nakanishi T, et al. Narrow-band phosphor $\text{K}_2\text{ZnP}_2\text{O}_7$: Eu^{2+} discovered using local structure similarity. *Scr Mater.* **2022**;215:114686. doi: [10.1016/j.scriptamat.2022.114686](https://doi.org/10.1016/j.scriptamat.2022.114686)
- [20] Dorenbos P. A review on how lanthanide impurity levels change with chemistry and structure of inorganic compounds. *ECS J Solid State Sci Technol.* **2013**;2(2):R3001–R3011. doi: [10.1149/2.001302jss](https://doi.org/10.1149/2.001302jss)
- [21] Dorenbos P. Energy of the first $4f^7-4f^6d$ transition of Eu^{2+} in inorganic compounds. *J Lumin.* **2003**;104(4):239–260. doi: [10.1016/S0022-2313\(03\)00078-4](https://doi.org/10.1016/S0022-2313(03)00078-4)
- [22] Hirosaki N, Takeda T, Funahashi S, et al. Discovery of new nitridosilicate phosphors for solid state lighting by the single-particle-diagnosis approach. *Chem Mater.* **2014**;26(14):4280–4288. doi: [10.1021/cm501866x](https://doi.org/10.1021/cm501866x)
- [23] Takeda T, Hirosaki N, Funahashi S, et al. New phosphor discovery by the single particle diagnosis approach. *Mater Discov.* **2015**;1:29–37. doi: [10.1016/j.md.2015.11.001](https://doi.org/10.1016/j.md.2015.11.001)
- [24] Takeda T, Hirosaki N, Funahashi S, et al. Narrow-band green-emitting phosphor $\text{Ba}_2\text{LiSi}_7\text{AlN}_{12}$: Eu^{2+} with high thermal stability discovered by a single particle diagnosis approach. *Chem Mater.* **2015**;27(17):5892–5898. doi: [10.1021/acs.chemmater.5b01464](https://doi.org/10.1021/acs.chemmater.5b01464)
- [25] Wang X, Takeda T, Hirosaki N, et al. Single-particle-diagnosis approach: an efficient strategy for discovering new nitride phosphors. *J Rare Earths.* **2018**;36(1):42–48. doi: [10.1016/j.jre.2017.08.006](https://doi.org/10.1016/j.jre.2017.08.006)
- [26] Takeda T, Funahashi S, Xie RJ, et al. Broadband white luminescent phosphor $\text{Ba}(\text{Si}_{7-x}\text{Al}_x)\text{Li}_y(\text{N}_{10-x+y}\text{O}_{x+y})$: Eu^{2+} with a high color rendering index for solid state lighting. *J Mater Chem C.* **2021**;9(16):5497–5504. doi: [10.1039/D0TC04228E](https://doi.org/10.1039/D0TC04228E)
- [27] Sheldrick GM. Shelxt – integrated space-group and crystal-structure determination. *Acta Crystallogr A.* **2015**;71(1):3–8. doi: [10.1107/S2053273314026370](https://doi.org/10.1107/S2053273314026370)
- [28] Sheldrick GM. Crystal structure refinement with SHELXL. *Acta Crystallogr C.* **2015**;71(1):3–8. doi: [10.1107/S2053229614024218](https://doi.org/10.1107/S2053229614024218)
- [29] Takahashi K, Takeda T, Hirosaki N. Luminescence of single-particle ceramic phosphor by proximity measurement. *Jpn J Appl Phys.* **2023**;62(1):016510. doi: [10.35848/1347-4065/acb2a2](https://doi.org/10.35848/1347-4065/acb2a2)
- [30] Takahashi K, Todoroki S, Takeda T, et al. Quantum efficiency measurement of single-particle phosphor by proximity method. *ECS J Solid State Sci Technol.* **2023**;12(7):076002. doi: [10.1149/2162-8777/ace0da](https://doi.org/10.1149/2162-8777/ace0da)
- [31] Xu J, Funahashi S, Takahashi K, et al. Cyan-emitting sialon-polytypoid phosphor discovered by a single-particle-diagnosis approach. *ECS J Solid State Sci Technol.* **2021**;10(11):116002. doi: [10.1149/2162-8777/ac331c](https://doi.org/10.1149/2162-8777/ac331c)
- [32] Hoerder GJ, Peschke S, Wurst K, et al. Polymorphs and derivatives of $\text{Sr}_2\text{LiAlO}_4$: Eu^{2+} . *Z Naturforsch B.* **2019**;74(10b):765–772.
- [33] Momma K, Izumi F. Vesta 3 for three-dimensional visualization of crystal, volumetric and morphology data. *J Appl Crystallogr.* **2011**;44(6):1272–1276. doi: [10.1107/S0021889811038970](https://doi.org/10.1107/S0021889811038970)
- [34] Bouquiaux J, Poncé S, Jia Y, et al. A first-principles explanation of the luminescent line shape of $\text{SrLiAl}_3\text{N}_4$: Eu^{2+} phosphor for light-emitting diode applications. *Chem Mater.* **2023**;35(14):5353–5361. doi: [10.1021/acs.chemmater.3c00537](https://doi.org/10.1021/acs.chemmater.3c00537)